Welding in the World (2022) 66:1535–1550
https://doi.org/10.1007/s40194-022-01308-2

RESEARCH PAPER

Ranking the susceptibility to hydrogen-assisted cracking in dissimilar metal welds

D. Bourgeois[1] · **B. Alexandrov**[1]

Received: 21 December 2021 / Accepted: 23 April 2022 / Published online: 13 May 2022

Abstract
Dissimilar metal welds (DMWs) are routinely used in the oil and gas industries for structural joining of high-strength steels to eliminate the need for post-weld heat treatment (PWHT) in field welding. Hydrogen-assisted cracking (HAC) can occur in DMWs during subsea service under cathodic protection. DMWs of two material combinations, 8630 steel/FM 625 and F22 steel/FM 625, produced with two welding procedures, non-temper bead (BS1) and temper bead (BS3), in the as-welded and PWHT conditions were investigated in this study. These DMWs were subjected to metallurgical characterization and testing with the delayed hydrogen cracking test (DHCT) to identify the effects of base metal composition, welding and PWHT procedures on their HAC susceptibility. The HAC susceptibility was ranked using the time to failure in the DHCT at loads equivalent to 90% of the base metal yield strength (YS) and the apparent stress threshold for HAC. A criterion for resistance to HAC in the testing conditions of DHCT was also established. The results of this study showed that 8630/FM 625 DMWs were more susceptible to HAC than the F22/FM 625 DMWs. PWHT did not sufficiently reduce the HAC susceptibility of the 8630/FM 625 and F22/FM 625 BS1 welds. DMWs produced using BS3 performed better than BS1 DMWs. The post-weld heat-treated F22/FM 625 BS3 DMW passed the HAC resistance criterion.

Keywords Dissimilar metal welds · Hydrogen-assisted cracking susceptibility · Delayed hydrogen cracking test

1 Introduction

DMWs are routinely used in the oil and gas industries for structural joining of internally clad high-strength low-alloy steel components to carbon steel pipes, aiming to eliminate the need of field post-weld heat treatment (PWHT). The high-strength steel components are overlaid with Ni-based filler metals and subjected to in-shop PWHT to meet the ASME code stress relief requirement and NACE heat-affected zone (HAZ) hardness requirement. The overlays, also named "butter welds," are then beveled, and field joined to carbon steel pipes using matching Ni-based welding consumables. The newly created HAZ is contained within the Ni-based weld overlay, thus eliminating the need for field PWHT of the final weld assembly. This study addresses the susceptibility to hydrogen-assisted cracking (HAC) of the dissimilar interface, between low-alloy steel components and Alloy 625 overlays / butter welds, shown in Fig. 1.

In-service failures of subsea oil and gas extraction systems, caused by hydrogen-assisted cracking (HAC) in DMWs, have resulted in extensive environmental damages and expensive repairs, shutdowns and loss of production. Hydrogen cracking theories were developed that aid in the understanding of how hydrogen behaves in metallic alloys [1–6]. Research has been conducted and reported on HAC mechanisms in weld overlays of low-alloy steels and corrosion-resistant alloys [7, 8]. Furthermore, there are review publications that bring together all the work performed and discuss paths forward to develop a unifying understanding of HAC and the hydrogen embrittlement phenomena [9–11].

There has been foundational research published that focuses on HAC in DMWs by various research institutions and oil and gas companies [12–18]. Brittle failures in DMWs of 8630 steel with FM 625 filler metal during subsea service under cathodic protection (CP) have been

Recommended for publication by Commission II - Arc Welding and Filler Metals

✉ D. Bourgeois
bourgeois.16@osu.edu

[1] Department of Materials Science and Engineering, Welding Engineering Program, The Ohio State University, Columbus, OH 43221, USA

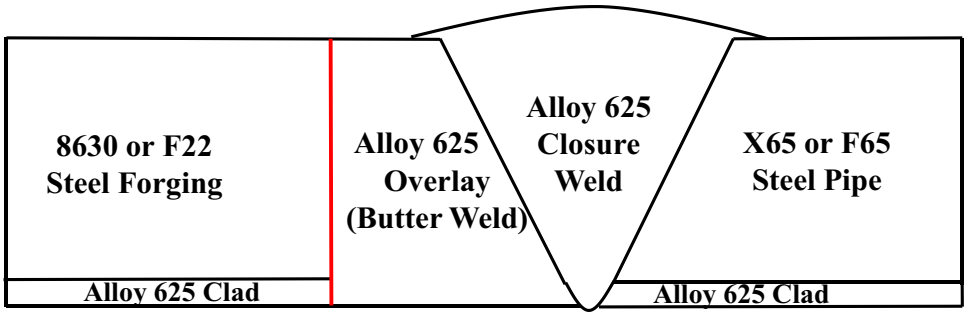

Fig. 1 Dissimilar metal weld assembly of internally clad low-alloy steel forging and low-alloy steel pipe using Alloy 625 butter and closure welds

reported by the oil and gas industry. These failures have been attributed to HAC due to local hydrogen embrittlement of susceptible microstructures that form at the fusion boundary during welding and PWHT [12, 19–22]. Currently, it is understood that the susceptibility to HAC is strongly affected by the base metal/filler metal combination, welding and PWHT procedures [12, 23]. Based on the current problem that HAC poses on DMWs, there is a need for a simple and reliable testing method, which can be utilized for evaluating HAC susceptibility in DMWs. The delayed hydrogen cracking test (DHCT) was developed at The Ohio State University [24, 25]. The DHCT is a testing method that allows simultaneous hydrogen charging and loading a sample with a constant tensile load. This testing method has been successful in ranking the susceptibility to HAC in F22 steel/FM 625 welds based on welding and PWHT procedures [25, 26]. The DHCT was used in this study to quantify and qualitatively rank the susceptibility to HAC in 8630 steel / FM 625 and F22 steel / FM 625 DMWs produced with two welding procedures in the as-welded and PWHT conditions.

2 Materials and procedures

2.1 Tested dissimilar metal welds

Two DMWs were subjected to metallurgical characterization and testing of HAC susceptibility this study: AISI 8630 / ERNiCrMo-3 and ASTM A182-F22 / ERNiCrMo-3. AISI 8360 and ASTM-A182-F22 are low-alloyed steels used in various oil and gas applications as pressure systems that include flanges, fittings, and valves. ER-NiCrMo-3 (FM 625) is an austenitic nickel-based alloy filler metal that is used as a weld overlay material due to its superior resistance to pitting and crevice corrosion cracking. The chemical composition of 8630 and F22 steels and FM625 is provided in Table 1.

The base metals were steel forgings of large pipe sections with inner diameter of 12 inches (304.8 mm) and wall thickness of 9 inches (228.6 mm). The 8630 steel forging was received in the quenched and tempered condition. The heat treatment procedure included normalizing at 1,607 ˚F (875 ˚C) and water quenching to 68 ˚F (20 ˚C), followed by tempering at 1256 F (680 ˚C) for 13 h and air cooling to ambient temperature. The F22 forging was normalized at 1750 ˚F (954 ˚C) and then air-cooled to the ambient temperature. Next, the forging was heated to 1300 ˚F (704 ˚C), tempered for 6 h and air-cooled to ambient temperature.

2.2 Welding procedures

Four forgings of each 8630 and F22 steel were overlaid with FM 625 using mechanized gas tungsten arc welding (GTAW) process with two different bead sequences as illustrated in detail in Figs. 2, 3 and 4. Prior to welding, the forging surface was machined and ground. Bead sequence describes the order in which the weld beads are laid in reference to the base material surface and are considered a component of the welding procedure. In bead sequence one (BS1) the weld beads are stacked normal to the surface of the steel substrate, Figs. 2a, 3a and 4a. In bead sequence three (BS3) the weld beads are laid along the substrate surface with 50% overlap between subsequent beads, Figs. 2b, 3b and 4b. Two forgings of each steel were overlaid using BS1 and two using BS3 welding procedures. The welding process and parameters used to manufacture the weld overlays are shown in Table 2.

Table 1 Chemical composition for 8630, F22 and FM 625

Material	Composition (Wt. %)										CE_{IIW}
	C	Mn	P	S	Si	Ni	Cr	Mo	Nb	Fe	
8630	0.32	0.93	0.008	0.003	0.35	0.82	0.97	0.41	0.004	Bal	0.806
F22	0.13	0.53	0.007	0.004	0.26	0.09	2.37	1.02	0.019	Bal	0.902
FM 625	0.018	0.01	0.005	0.004	0.36	64.42	21.27	8.74	3.28	1.82	

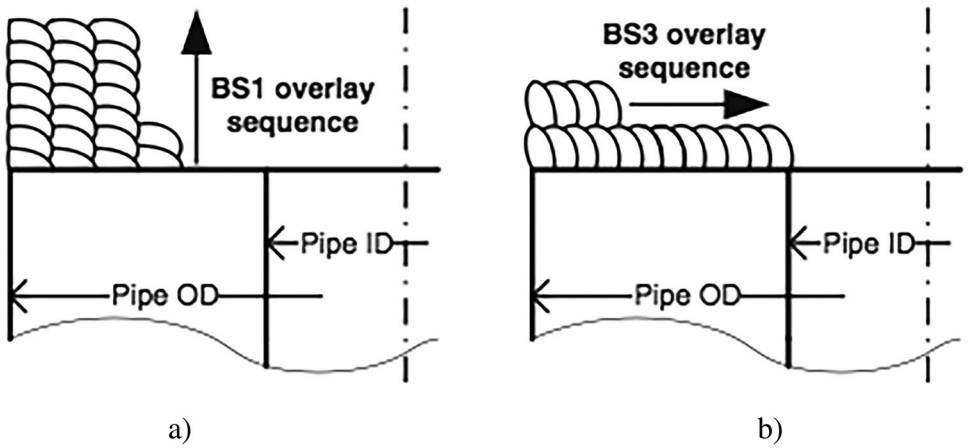

Fig. 2 Welding overlay bead sequences: **a**) BS1 and **b**) BS3 [12]

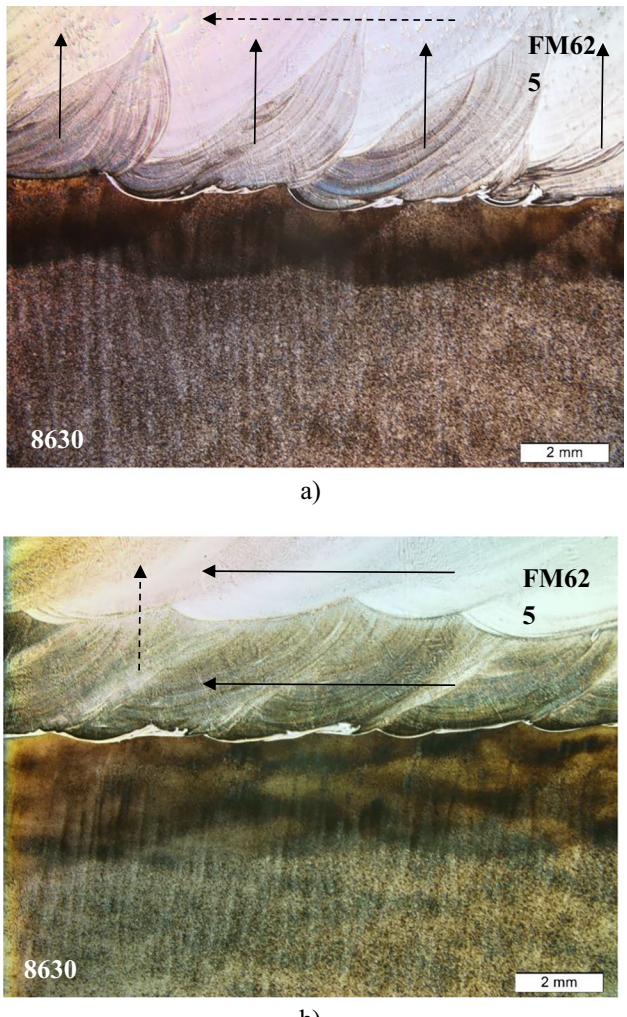

Fig. 3 Macro-sections of the tested 8630 / FM625 DMWs: **a**) stacking bead sequence BS1, **b**) overlapping bead sequence BS3. Solid line arrows identify bead sequence, and dashed line arrows identify layer sequence

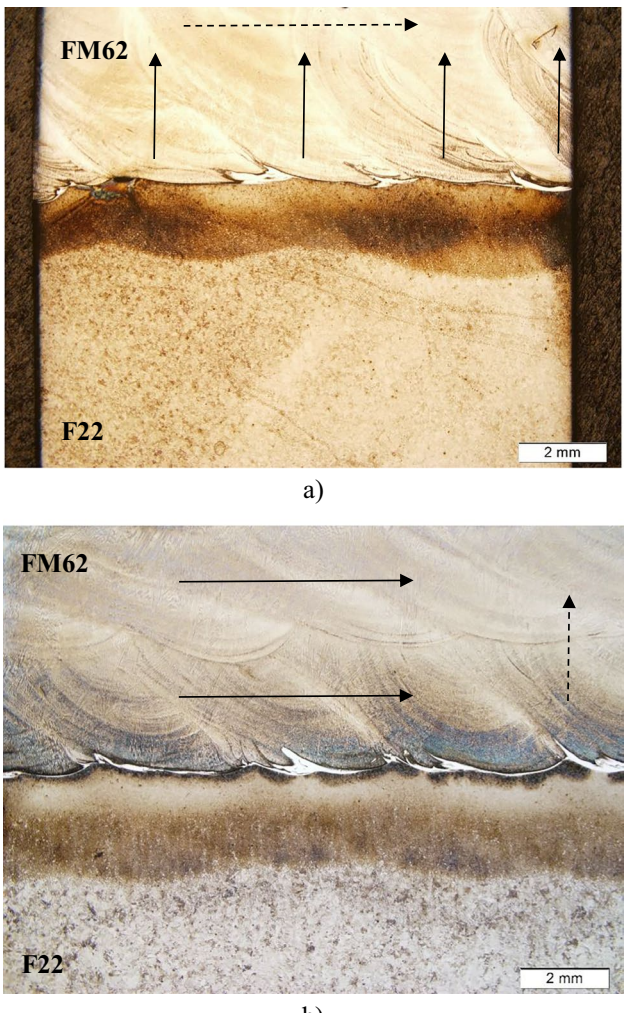

Fig. 4 Macro-sections of the tested F22 / FM625 DMWs: **a**) stacking bead sequence BS1, **b**) overlapping bead sequence BS3. Solid line arrows identify bead sequence, and dashed line arrows identify layer sequence

Table 2 Gas tungsten arc welding process for production of FM 625 overlays on 8630 and F22 steel forgings

Base Material	Mod AISI/SAE 8630/ASTM A182-F22
Wall thickness	2.75 in (69.85 mm)
Surface preparation	Machine ground
Transfer mode	Stringer
Filler material	ERNiCrMo-3 (FM 625)
Wire diameter	0.125 in (3.175 mm)
Preheat	400 _F minimum (204 _C); 600 °F maximum (316 °C)
Gas	Argon
Position	1G BS3; 2G BS1
Travel speed	8.0 in/min (203 mm/min)
Current	178 – 183 A
Voltage	10.7 -11.4 V
Heat input	14.6 – 15.5 kJ/in (0.57 kJ/mm)

Fig. 5 DHCT frames setup

After welding, one BS1 and one BS3 overlays on each 8630 and F22 steel forgings were subjected to PWHT for 10 h at 1202 °F (650 °C), which is an industry standard stress relief heat treatment. The other BS1 and BS3 weld overlays on 8630 and F22 steel forgings were left in the as-welded condition. The latter were produced on forgings that were previously heat-treated for 10 h at 1202 °F (650 °C). The combined welding and PWHT procedures produced four different weld overlays in each of the 8630 and F22 steels: as-welded BS1 and BS3, and post-weld heat-treated BS1 and BS3. Macrographs of the as-welded 8630/FM 625 and F22/625 BS1 and BS3 overlays are shown in Figs. 3 and 4.

2.3 Evaluation of hydrogen-assisted cracking susceptibility

The DHCT [24, 25] was used to evaluate and rank the HAC susceptibility in both overlays in the as-welded condition and after PWHT. The DHCT allows simultaneous hydrogen charging and constant tensile loading. The full DHCT setup is shown in Fig. 5. Sample elongation is measured during testing via a linear variable differential transformer (LVDT). The LVDT is positioned at the end of the loading arm, and the LVDT signal is recorded using a personal computer. The LVDT records are used to determine the time of failure for tested samples. The hydrogen charging was performed at current density of 10 mA/cm^2 in electrolyte composed of 0.1 normal solution of sulfuric acid (H_2SO_4) in distilled water plus 0.1 g/l of sodium thiosulfate ($Na_2S_2O_3$). The testing was performed at room temperature with continuous recirculation of the electrolyte via peristaltic pumps and stirring devices (in 5-gallon electrolytic containers) to aid in maintaining a constant pH throughout testing. Figure 6 shows the DHCT test cell, including the electrolytic charging circuit and a test sample under constant tensile load.

The HAC susceptibility in all tested DMWs was ranked by determining the time-to-failure (TTF) in the DHCT at tensile loads corresponding to 90% of the specified minimum yield strength of the base metal in the normalized and tempered condition. The apparent threshold for HAC was determined by testing the DMWs subjected to PWHT to a series of lower tensile loads. NACE TM0177 defines apparent threshold stress for environmental cracking as the maximum no-failure stresses for a specified exposure period [29]. In this study, the apparent threshold stress for HAC was defined as the maximum stress which DMW test samples can withstand without failing the DHCT for a duration longer than needed for full saturation with hydrogen (see Sect. 3.2).

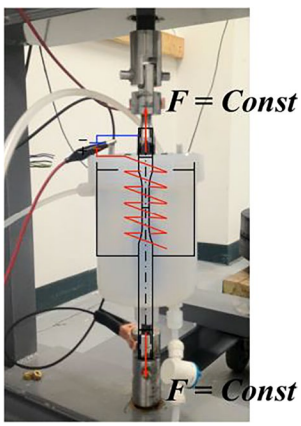

Fig. 6 DHCT test cell illustrating constant tensile load application and electrolytic charging with hydrogen

2.4 Test samples

The test sample geometry used in this study was different from traditional "dog-bone" samples and was developed to ensure that the DHCT method would produce reliable and repeatable results. The sample design is shown in Fig. 7, and the sample dimensions are listed in Table 3. The primary focus for the final test sample geometry was to minimize stress concentration in the gauge section, incorporate more welding beads of production welds and maintain a uniform stress distribution at the fusion boundary. Potential local overcharging with hydrogen at sharp corners, which may affect the location of crack nucleation, is avoided by utilizing rounded edge gauge section (R1 in Fig. 7).

The DHCT sample design was optimized using computer aided design (CAD) and finite element analysis (FEA) software. Figure 8 illustrates how the radius at the front face of the DHCT sample was optimized to ensure uniform stress concentration factor (SCF) at the gauges section. The FEA for the DCHT sample design optimization was performed by Justin Crapps of the ExxonMobil Corporation Upstream Research Company.

The DHCT samples were machined by wire cut electro discharge machining (EDM), which allowed for the complex geometry of the sample to be produced. The samples were extracted with the fusion boundary located in the middle of the gauge section and oriented normal to the welding direction, Fig. 9. Before testing, the gauge section was manually polished with 600-grit sandpaper to remove the surface oxide layer produced by EDM. After the removal of the surface oxide layer, the sample was rinsed with ethyl alcohol and dried to remove excess moisture. During testing, the dissimilar fusion boundary and a 10-mm-wide area of the low-alloy steel side of the gauge section were exposed to hydrogen charging. The unexposed part of the test sample was protected by a rubber coating.

Table 3 DHCT sample dimensions

Dimension	Size	
	in	mm
B	0.10 ± 0.002	2.54 ± 0.05
C	0.75 ± 0.002	19.05 ± 0.05
E	2.4 ± 0.002	60.96 ± 0.05
F	0.375 ± 0.002	9.53 ± 0.05
G	3.0 ± 0.005	76.2 ± 0.13
H	1.95 ± 0.002	24.13 ± 0.05
I	0.4—0.020	10.09—0.05
J	0.55 ± 0.002	13.97 ± 0.05
D1	0.25 + 0.005	6.35 ± 0.13
R1	0.05 ± 0.002	1.27 ± 0.05
R2	0.02 ± 0.002	0.51 ± 0.05
R3	0.01 ± 0.002	0.254 ± 0.05
R4	0.5 ± 0.005	12.7 ± 0.13

2.5 Metallurgical characterization

Samples of the tested DMWs were prepared for examination using standard metallography procedures. The F22 steel–FM 625 and 8630 steel–FM 625 welds had a combination of two etchants that were applied to reveal the microstructures of each respective base metal. First, a 2% Nital acid mix was applied to reveal the F22 and 8630 microstructures of the weld by full submersion of the sample in the etchant for 5 – 20 s. The application the Nital etch first allows for protection of the steel during the chromic etch. Next, the sample was placed into a 10%

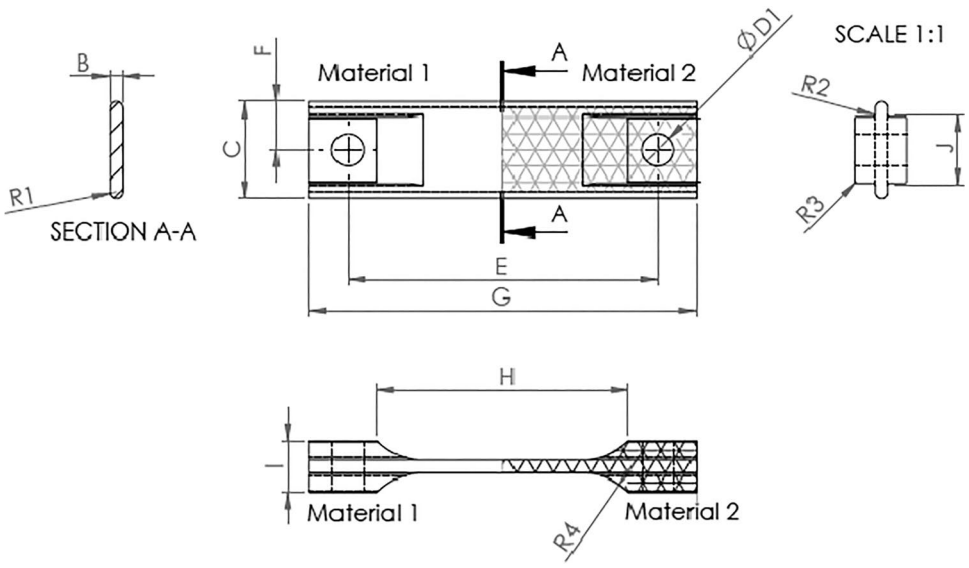

Fig. 7 DHCT sample design

chromic etchant. Five (5) volts was applied to the sample over the Alloy 625 material by using a tungsten electrode, which was placed directly on the sample and a stainless steel foil as the anode that was placed over the sample but submerged slightly in the etch. The voltage administered for 5 s. After the chromic etch was applied, the sample was observed using the light optical microscope to ensure that adequate etching was applied for metallurgical characterization. Then, the chromic etchant was completely cleaned from the sample by immersing in an ethanol bath, followed by rinsing with water and ultrasonic cleaning. Table 4 highlights the chemical composition and technique of the etchants that were used for metallurgical characterization.

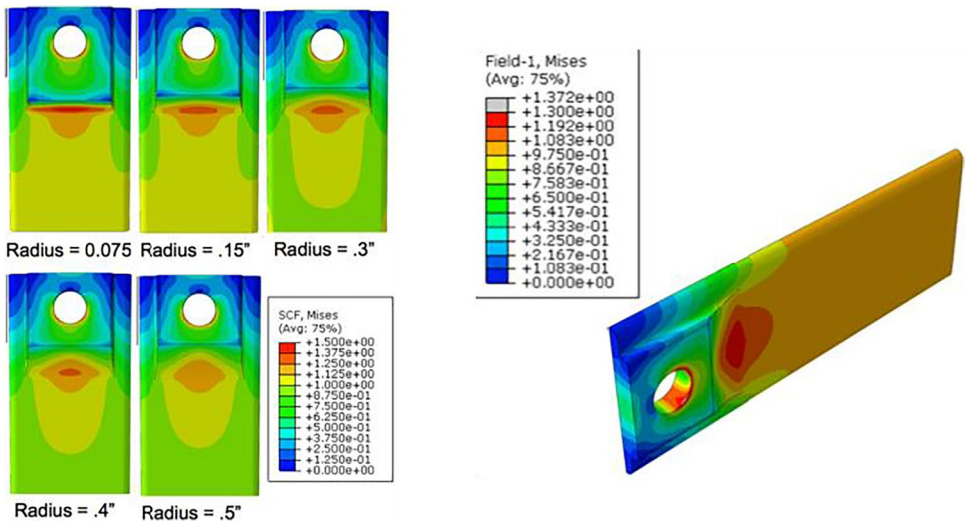

Fig. 8 FEA models of the varying front face radius with respect to SCF (left) and FEA model showing uniform Von Mises stress across the gauge section (right)

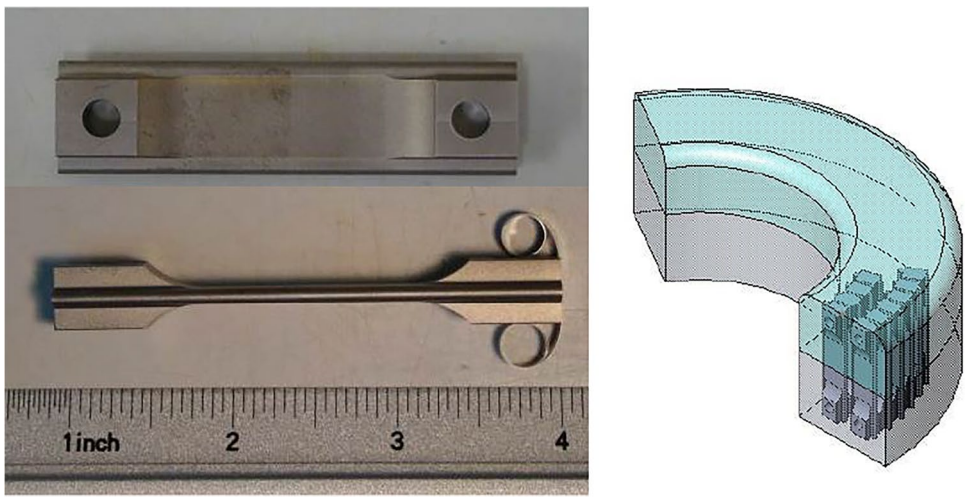

Fig. 9 DHCT sample design and extraction schematics

Table 4 Etchants composition and techniques used for metallographic characterization

Etchant	Material	Composition	Technique
10% Chromic (CrO_3^+)	F22/8630 – FM 625 welds	CrO_3 (20 g) H_2O (180 mL)	Submerge completely in solution and etched at 5 V for 5 s using tungsten cathode, stainless steel anode
2% Nital	F22/8630 – FM 625 welds	HNO_3 (1 mL) Ethanol (50 mL)	Submerge completely in solution for 5 – 20 s

A low-angle micro-sectioning (LAMS) technique [12], which involves sectioning of DMWs at a low angle relative to the fusion boundary, was utilized for detailed examination of the narrow dissimilar transition zone. The compositional gradients across the dissimilar transition zone were quantified using energy-dispersive spectroscopy (EDS) within a scanning electron microscope (SEM) at 25 – 30 kV with a 3 – 5 µm spot size with a working distance of 9 – 10 mm.

3 Results

3.1 Fusion boundary region microstructure

The microstructures that are formed in the dissimilar transition zone of DMWs are complex and span across a localized area along the fusion boundary [12, 25]. It is important to identify the microstructure and quantify the gradients of composition and mechanical properties in the fusion boundary region in relation to the HAC susceptibility of DMWs. In addition, the metallurgical characterization results will be used for estimation of the hydrogen diffusion parameters and hydrogen saturation time of DHCT samples in the establishment of tentative criterion for HAC susceptibility.

The fusion boundary region in the tested DMWs includes the coarse-grained heat-affected zone (CGHAZ), a region of planar growth solidification at the fusion boundary that transitions into cellular dendritic and columnar dendritic solidification, and swirls of base metal partially diluted with the Alloy 625 filler metal, Figs. 10, 11 and 12. The dilution profiles of the planar growth region and the swirls, shown in Figs. 13 and 14, were calculated using the iron content profile from EDS traverses across the fusion boundary.

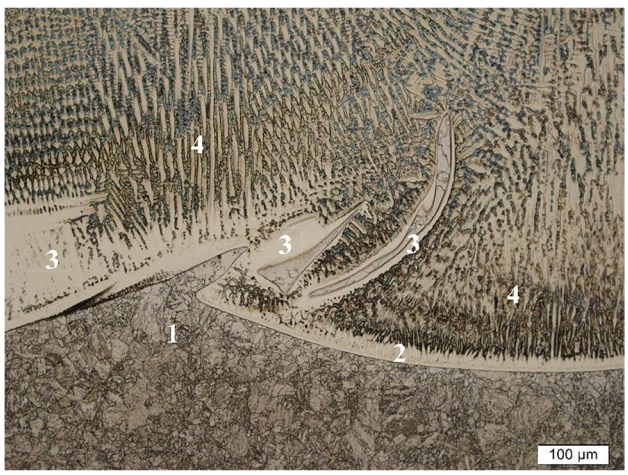

Fig. 10 Typical microstructure in the fusion boundary region of the tested DMWs: 1 – CGHAZ, 2 – planar growth and cellular dendritic regions, 3 – swirls, 4 – columnar dendritic weld microstructure (as welded F22 BS3)

a)

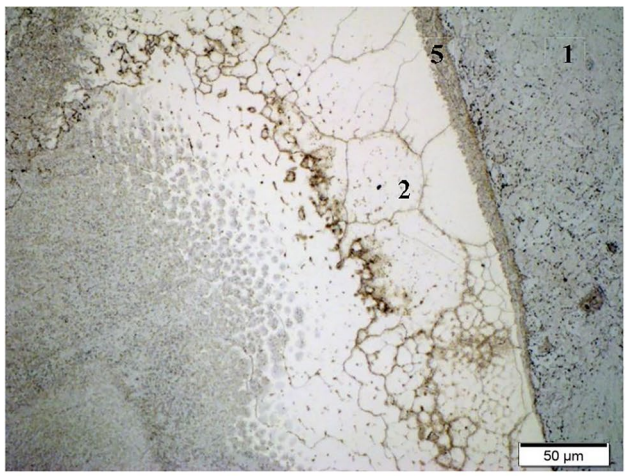

b)

Fig. 11 **a**) 8630 BS1, **b**) LAMS of F22 BS3. Typical planar growth region microstructure: 1 – CGHAZ, 2 – planar growth region, 3 – cellular dendritic region, 4 – columnar dendritic weld, 5—PMxZ at the fusion boundary

In the as-welded condition, the CGHAZ microstructure in the tested DMWs was predominantly composed of fresh martensite with hardness values exceeding 480 HV_{10} in 8630 steel and 425 HV_{10} in F22, Figs. 15 and 16. The bead overlap BS3 welding procedure generated a strong tempering effect, resulting in significant reduction in the as-welded CGHAZ hardness, Fig. 16. PWHT reduced the CGHAZ hardness to levels close to or below the 250 HV_{10} requirement of NACE MR0175 for cracking resistance in H_2S environments [26].

The planar growth region exhibited very steep dilution profile next to the fusion boundary and a width varying in a range of approximately 5 µm to 50 µm, Fig. 10 through Fig. 13. This region exhibited steep compositional gradient of 94% to 24% dilution and had austenitic microstructure with low hardness in the as-welded condition, Figs. 13

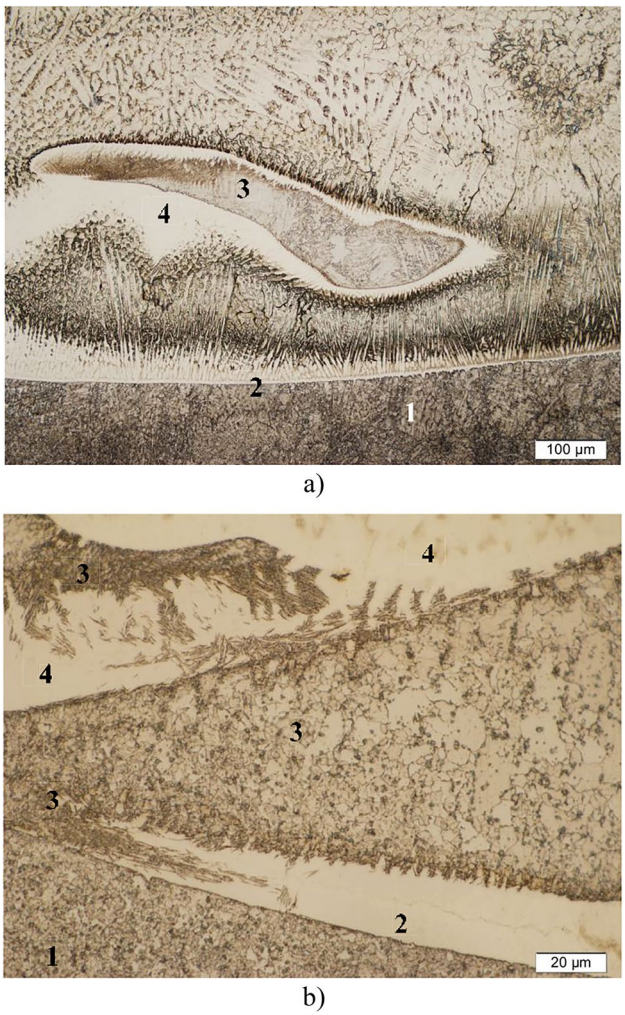

Fig. 12 **a**) 8630 BS1, **b**) LAMS of 8630 BS3. Typical swirl microstructure: 1 – CGHAZ, 2 – planar growth region, 3 –PMxZ within a swirl, 4 –planar growth region within a swirl

and 15. PWHT resulted in formation of local hard zones in the 8630 DMWs exceeding 450 HV_{10}, Fig. 16.

Utilization of a LAMS technique allowed visualizing narrow partially mixed zones (PMxZs) that are present along the dissimilar fusion boundary, Fig. 11b. The PMxZs are composed of base metal partially mixed with FM625 and have martensitic microstructure [28]. The swirls found along the dissimilar fusion boundary had dilutions in the range of 97% to 70%, Fig. 14. The swirls contained PMxZs of high dilution and planar growth regions of low dilution, with compositions close to the base metal and the filler metal, respectively, Figs. 12 and 14. The swirls' PMxZs had hardness in the range of 300 to 420 HV_{10} in both the as-welded and PWHT conditions, Fig. 15. The width of typical weld metal swirls varied between 100 µm and 200 µm.

3.2 Development of tentative criterion for HAC resistance of DMWs

This study established a tentative criterion for defining the resistance to HAC in DMWs, which is based on test results from the DHCT. Resistance to HAC was defined as sustaining the DHCT without failure under constant tensile load, equivalent to 90% of the base metal yield strength (YS), for a duration longer than the time for hydrogen saturation of the DMW tested sample. This criterion reflects the DHCT procedure, in terms of constant tensile load and continuous charging with hydrogen, and accounts for the three major controlling factors of the HAC phenomenon in metallic alloys: susceptible microstructure, applied tensile stress in the elastic range, and sufficient hydrogen concentration. In the DHCT, the effect of microstructure is accounted for through its HAC resistance and through its effect on the kinetics of hydrogen saturation.

Previous research has identified microstructural constituents in the fusion boundary region of DMWs that are susceptible to HAC. These include: 1) hard martensitic microstructure in the CGHAZ in the as-welded condition, 2) hard planar growth region that exhibits peak hardness after PWHT, and martensitic PMxZs located along the fusion boundary and in swirls [12, 23, 25, 26, 30]. The metallurgical characterization results presented in Sect. 3.1 demonstrated that all these microstructural constituents were present in the tested DMWs.

The hydrogen saturation path of the fusion boundary region in a DHCT sample is defined by the exposed surface of the sample and by the sample thickness, Fig. 7. It can be assumed that hydrogen atoms would saturate the CGHAZ by diffusion through the sample surface and through the adjacent base metal. The CGHAZ would than serve as a source of hydrogen for saturation of brittle microstructures at the fusion boundary and of PMxZs located in swirls. Therefore, time for saturation with hydrogen of the HAC susceptible microstructures at the fusion boundary region can be determined as follows:

$$t_s = t_{CGHAZ} + t_{swirls} \quad (1)$$

where t_s, t_{CGHAZ} and t_{swirls} are, respectively, the times for saturation with hydrogen of the entire fusion boundary region, the CHGAZ, and the swirls. The hydrogen saturation times were calculated using published database of hydrogen diffusion coefficients compiled by Bollinghaus et al. [27] and a simplified diffusion relationship:

$$t = l^2/D \quad (2)$$

where D in the hydrogen diffusion coefficient in mm^2/sec, l is the diffusion distance in mm and t is hydrogen charging duration in seconds.

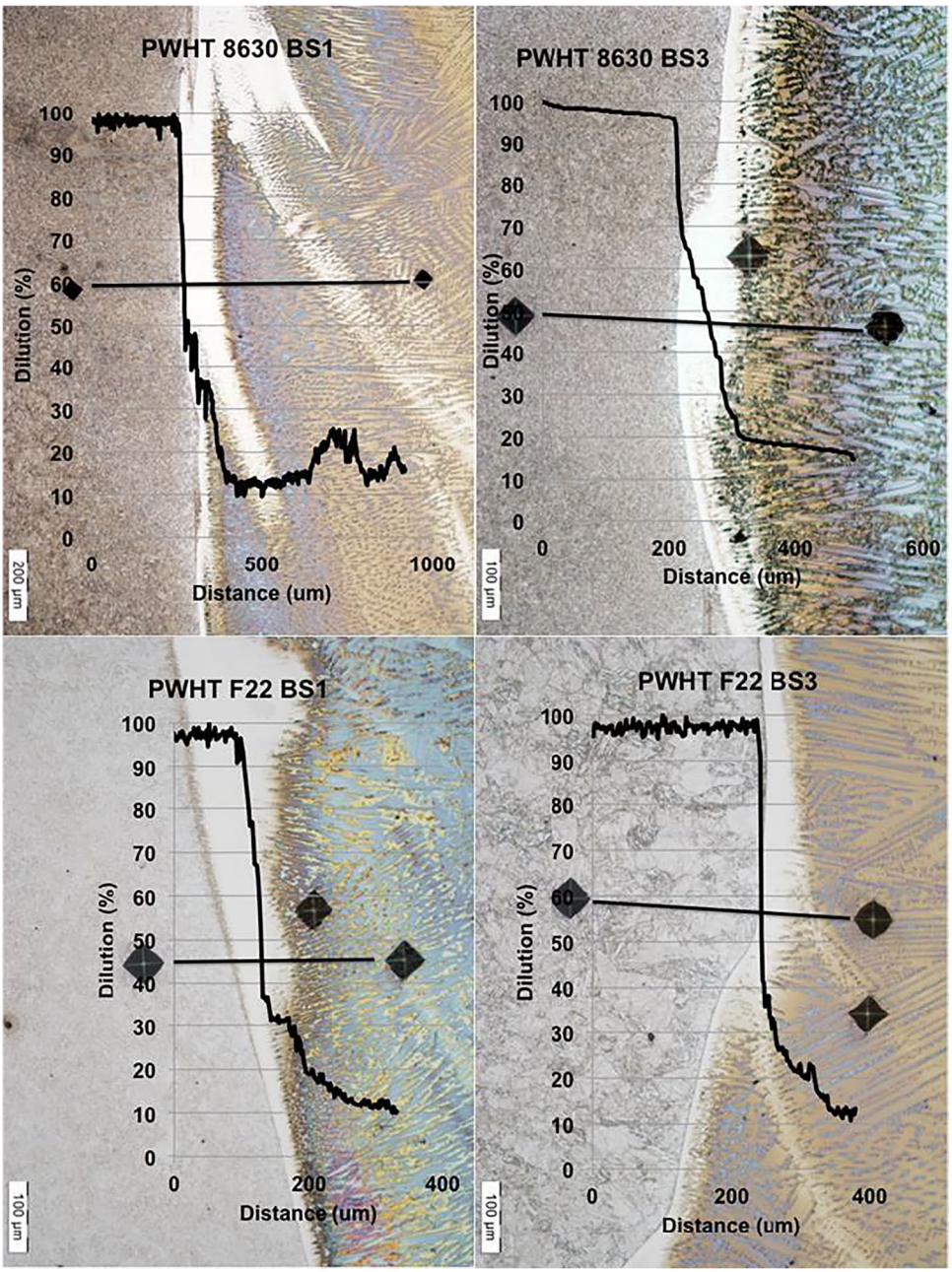

Fig. 13 Typical microstructure in the fusion boundary region and dilution profile of the planar growth region

A range of room temperature diffusion coefficients for martensitic microstructures in low-alloy steels, selected from the diffusion database, and a diffusion distance equal to half of the sample thickness, 1.27 mm, were used for the saturation time calculation in the CGHAZ, Table 5. The saturation time in the planar growth region and in swirls was calculated using a range of diffusion coefficients for high-alloyed ferritic and austenitic steels and a diffusion distance of 200 µm, corresponding to typical swirls lengths determined in Sect. 3.1. The selected ranges of diffusion coefficients and the diffusion distances would be representative for the hydrogen saturation of DHCT samples in DMWs with wide range of base metal / filler metal combinations.

The estimated minimum and maximum times for full saturation with hydrogen of a DHCT sample were, respectively, 55.9 and 559 h. A conservative non-failure criterion of 1,120 h, for testing of DMWs with the DHCT, was established by implementing a safety factor of 2 over estimated maximum saturation time of 560 h. Factors such as plastic strain accumulation that influences dislocation motion and would lead to faster hydrogen diffusion were not accounted for in estimating the time for hydrogen saturation.

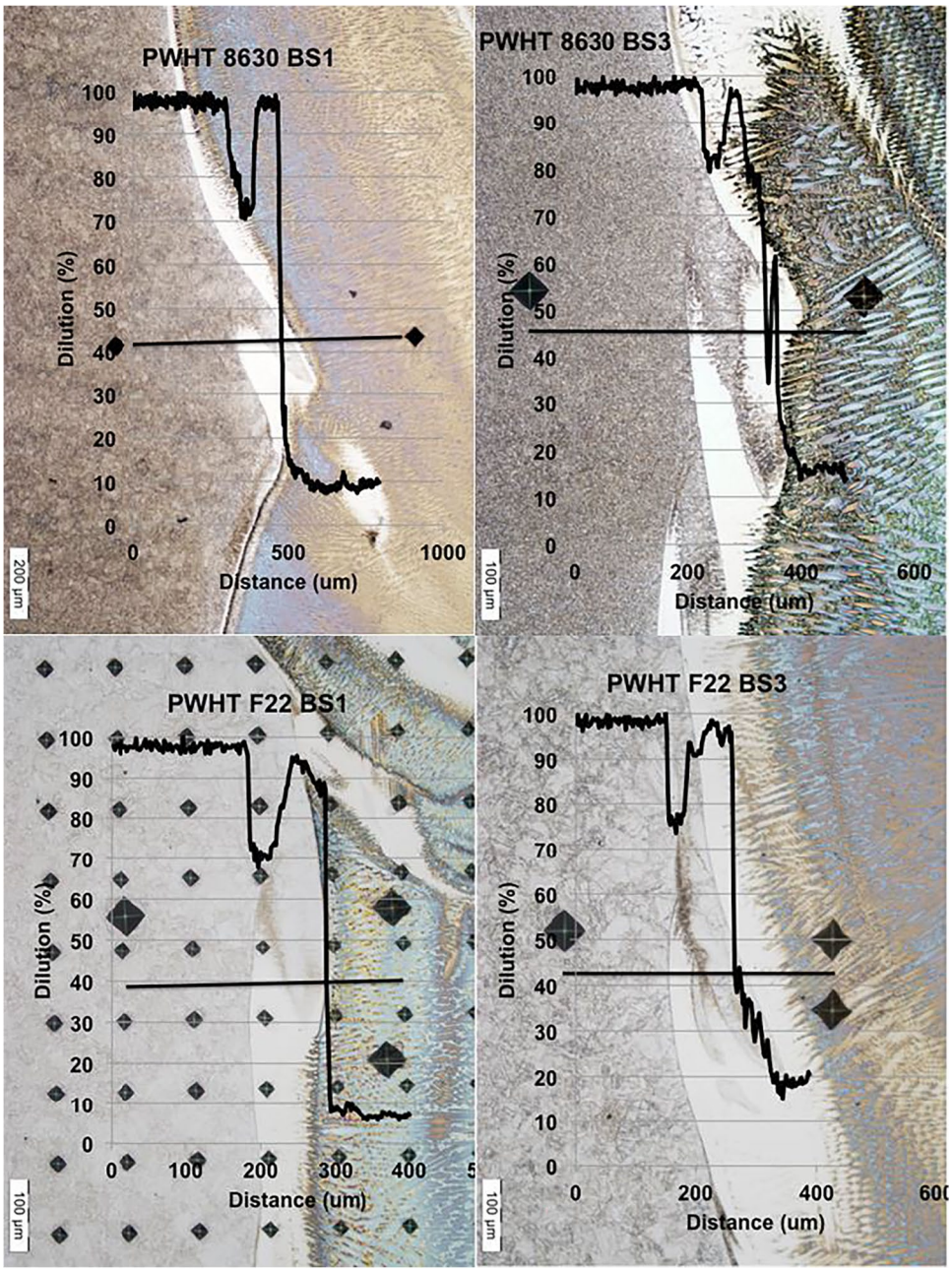

Fig. 14 EDS traverse across weld metal swirls in PWHT 8630- and F22-FM 625 BS1 and BS3

3.3 Quantification of hydrogen-assisted cracking susceptibility in dissimilar metal welds

The DHCT results are summarized in Table 6 and Figs. 17 and 18. All tested samples experienced brittle failures in the fusion boundary region. The dashed horizontal and vertical lines in Fig. 18 identify: 1) the 90% YS load time-to-failure criterion for HAC susceptibility ranking and 2) the 1,120 h no-failure at 90% YS load criterion for resistance to HAC. Based on these criteria, the F22/625 BS3 PWHT weld can be classified as resistant to HAC. The 8630/625 DMWs are ranked as the most susceptible to HAC, followed by the F22/625 BS1 welds and the F22/625 BS3 as-welded. PWHT did not reduce the HAC susceptibility in the 8630/625 BS1 weld, provided some reduction in HAC susceptibility of the 8630/625 BS3 and F22/625 BS1 welds and completely mitigated the HAC susceptibility in the F22/625 BS3 weld. Welding procedure BS3 had stronger effect on improving the HAC resistance in the F22/625 welds than in the 8630/625 welds.

Apparent threshold stress of HAC was determined for post-weld heat-treated F22/625 BS1 and BS3 welds, which respectively sustained DHCT loads of 265 MPa (60% YS) and 508 MPa (115% YS) without failure for more than

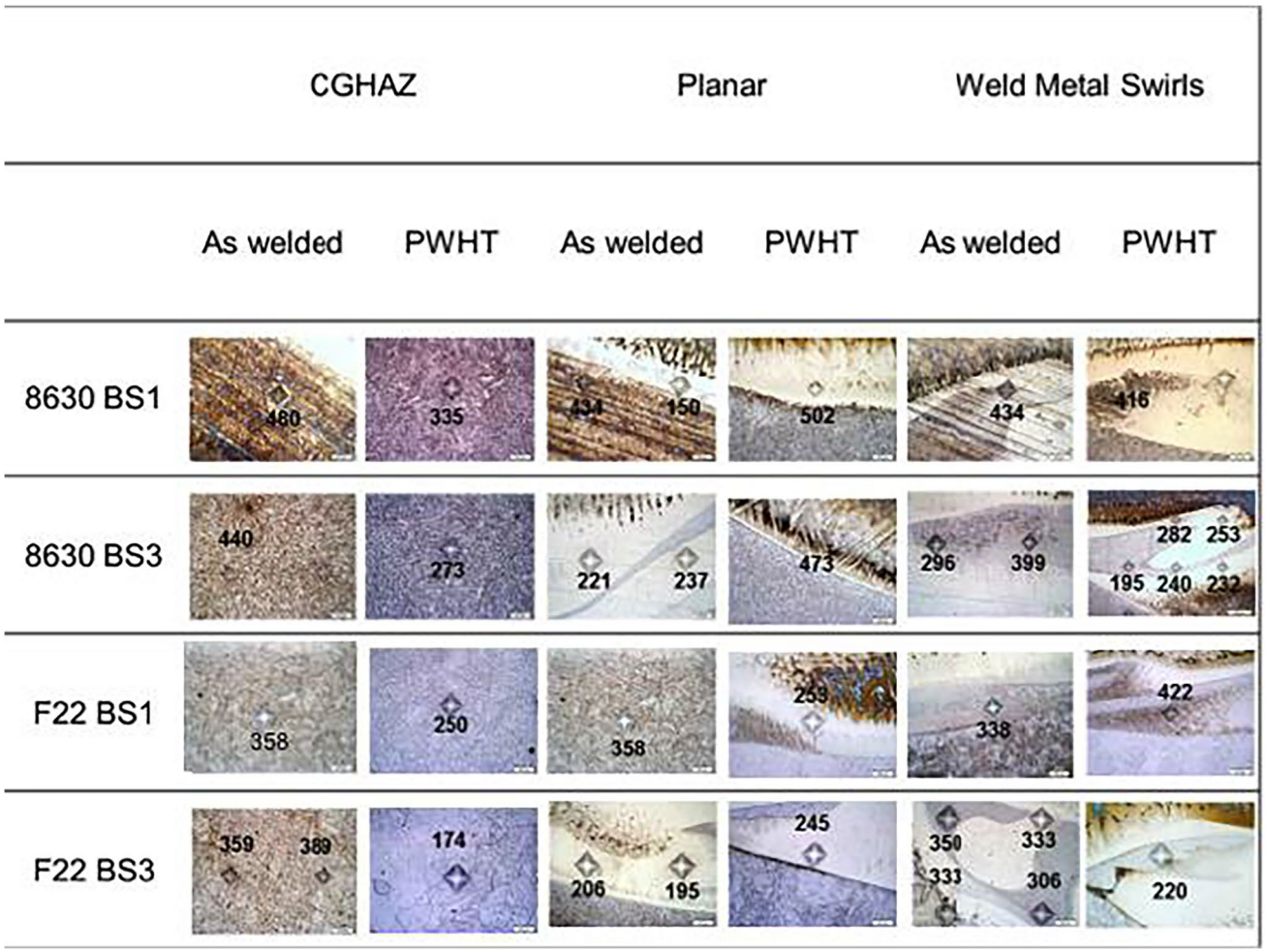

Fig. 15 Microstructure and typical hardness values in the CGHAZ, planar growth region, and swirls of the tested DMWs

1,200 h. Apparent threshold stress was not determined for the post-weld heat-treated 8630/625 BS1 and BS3 welds that failed the DHCT respectively after 285 h at 224 MPa (40% YS) and after 250 h at 444 MPa (50% YS). The low failure stresses and short times to failure, shorter than the estimated time for full saturation with hydrogen of 560 h, suggested very low apparent threshold stresses of these welds, potentially below 40% YS, that did not justify further testing.

4 Discussion

The results of this study show a wide range of HAC susceptibility in the tested DMWs, demonstrated by 1) times to failure ranging between 0.1 and 839 h and no failure for more than 1,200 h at loads of 90% YS and 2) apparent threshold stresses varying between lower than 40% YS and up to 115% YS. These results evidence a strong effect of the base metal composition, welding and PWHT procedures on the microstructure and HAC susceptibility in the tested DMWs, as well as a high sensitivity of the DHCT for the effect of these factors.

The high HAC susceptibility in the as-welded condition of both 8630/FM 625 and F22/FM 625 DMWs is related to formation of large amounts of hard martensite in the CGHAZ, evidenced in the hardness maps in Fig. 16 and in the hardness frequency distribution charts in Fig. 19. High hardness values, approaching the CGHAZ hardness, were found in the PMxZs located at the fusion boundary and in weld metal swirls, Figs. 11, 12 and 15. The PMxZ are formed by high dilution of molten base metal in the FM625 weld pool, resulting in alloy steel compositions with high hardenability that form hard martensitic microstructures [12, 30]. Compared to F22, the higher carbon content in the 8630 steel resulted in significantly higher CGHAZ and PMxZ hardness, Figs. 15, 16 and 19a, and shorter times to failure, Table 5 and Fig. 17.

The welding procedures, represented by bead sequences BS1 and BS3, have a strong effect on the HAZ microstructure. By staking weld beads vertically relative the substrate

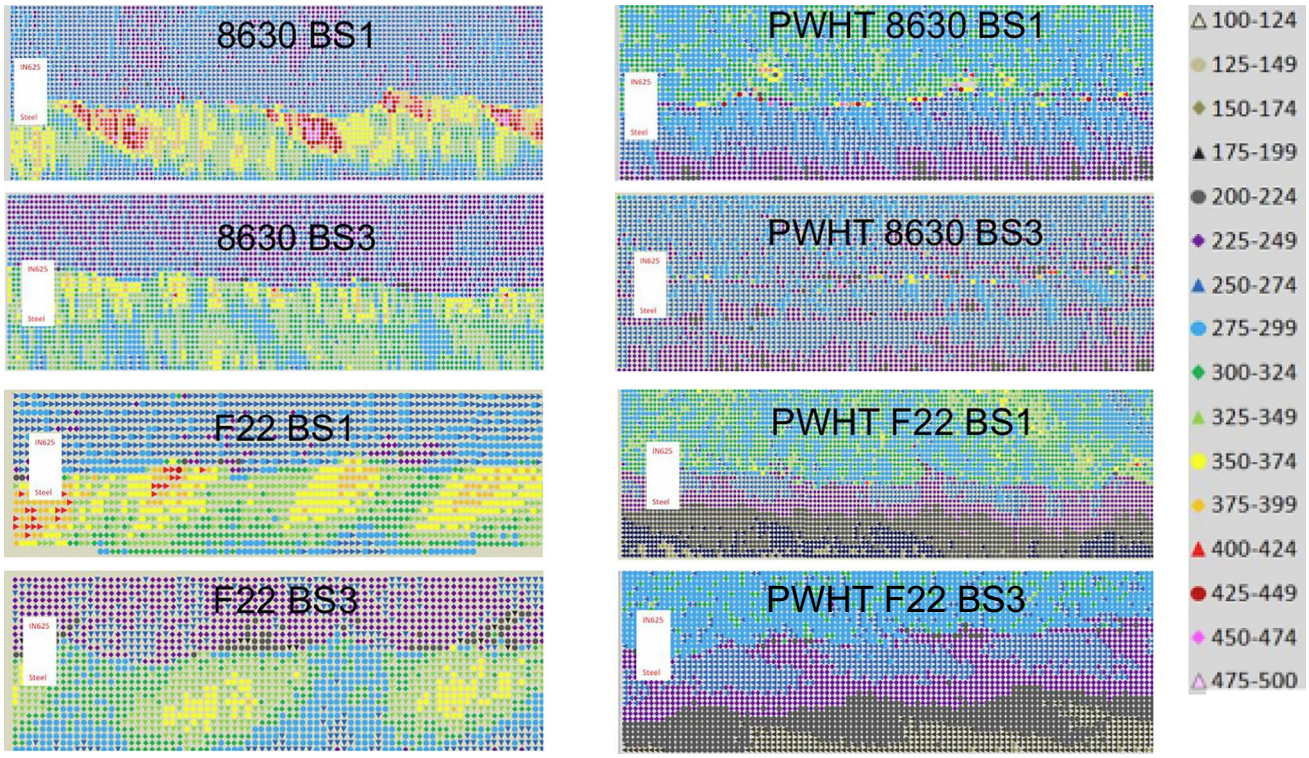

Fig. 16 Hardness maps in the fusion boundary region of tested DMWs, HV0.1, 100 um step

surface, BS1 provides conditions for lower interpass temperatures, resulting in formation of larger swirls, faster cooling rates, and higher hardness in the CGHAZ. BS1 also creates sharp bead toe angles at the substrate surface, which are difficult to penetrate by subsequent weld beads and frequently lead to formation of lack of fusion defects. Such lack of fusion defects, located in the fusion boundary region of DMWs, serves as HAC nucleation sites [31].

The overlapping beads in procedure BS3 tempered the CGHAZ of the preceding beads, significantly reducing the overall CGHAZ hardness, Fig. 16. In the as-welded condition, there is a bimodal hardness distribution in both DMWs: a more concentrated distribution in the lower hardness range pertaining to the weld metal and a wider distribution in the higher hardness range pertaining to the CGHAZ, Fig. 19a. The hardness frequency distribution clearly demonstrated the effect of CGHAZ tempering generated by BS3. The bead sequence did not have a significant effect on the HAC susceptibility in the as-welded 8630/625 DMWs, Fig. 17, since both BS1 and BS3 had very high CGHAZ hardness, exceeding 460 HV_{10}, Figs. 15 and 19a. In the F22/625 welds, however, BS3 reduced the maximum CGHAZ hardness below 390 HV_{10}, which increased the time to failure with one order of magnitude.

PWHT reduced the maximum CGHAZ hardness in the 8630 and F22 steels below 300 HV_{10} and 275 HV_{10}, respectively, Fig. 16. However, the PWHT resulted in significant hardness increase in the narrow dissimilar transition zone in both 8630/FM 625 DMWs and in the F22/FM 625 BS1 weld. This phenomenon is related to carbon migration from the CGHAZ towards the dissimilar transition zone, resulting in carbon accumulation and carbide precipitation in the planar growth region [12, 22]. Thermodynamic and kinetic simulations of carbon behavior during PWHT, validated using electron probe micro analysis [12], have predicted carbon accumulation in the planar growth region of 8630/FM 625 DMWs in the order of 1.2 to 1.8 wt.% [12, 31, 32] and up to 0.7 wt.% in F22/FM 625 DMWs [26, 31]. The carbon migration during PWHT of ferritic steel / Ni-base DMWs is caused by the steep gradient of the chemical potential of carbon at the dissimilar interface [12, 31, 32]. The higher carbon and lower carbide formers content in 8630 steel resulted in a larger driving force for carbon migration and harder planar

Table 5 Calculation of the hydrogen saturation time in DHCT samples

Range	D_{CGHAZ} (mm^2/sec)	D_{swirl} (mm^2/sec)	l_{CGHAZ} (mm)	l_{swirl} (mm)	Saturation Time, t_S (hours)
min	1*10e-5	1*10e-6	1.27	0.2	55.9
max	1*10e-6	1*10e-7	1.27	0.2	559

Table 6 DHCT test results

Sample	% YS	Load (MPa)	TTF (hrs)
8630 BS1 AW	90	583	1.0
			0.1
8630 BS1 PWHT	104	583	0.8
	90	505	0.5
	80	449	0.7
	70	393	1.8
	60	337	154.9
	50	281	387.0
	40	224	284.9
8630 BS3 AW	90	583	0.2
			0.1
8630 BS3 PWHT	117	583	0.6
	95	474	1.2
	92.5	462	0.8
	92.5	462	1.8
	90	449	1.6
	80	399	4.0
	70	349	3.0
	60	299	256.5
	50	250	444.2
F22 BS1 AW	90	508	3.4
F22 BS1 PWHT	115	508	7.8
	90	398	38.6
			90.1
	80	354	167.9
	70	309	839.0
	60	265	1213 NF
F22 BS3 AW	90	508	39.4
F22 BS3 PWHT	115	508	1316.9 NF
	90	401	1248.0 NF

growth region in 8630/FM 625 DMWs, compared to the F22/FM 625 welds, Figs. 15 and 16.

The welding procedures also affected carbon migration during PWHT. The bead tempering procedure BS3 generated stable carbides in the CGHAZ, reducing the driving force for carbon migration and the planar growth region hardness, Figs. 15 and 16. This effect was stronger in the F22/625 DMW, where the lower carbon content and higher content of carbide formers, Cr and Mo, essentially prevented hardening in the planar growth region.

Previous research [12, 32] and the results in this study show that PWHT did not reduce the hardness in PMxZs, Fig. 15. The high Ni content in PMxZs could reduce their A_3 and/or A_1 temperatures below the PWHT temperature leading to austenitization during PWHT and formation of fresh martensite on cooling to room temperature. Thermodynamic simulations have demonstrated that increasing Ni content to 12 wt.% in PMxZs composed of 8630 steel and Alloy 625 filler metal resulted in reduction of the A1 and A3 temperatures respectively with about 200 °C and 150 °C [12].

Figure 19b illustrates the combined effect of PWHT and welding procedure on the hardness distribution of the tested DMWs, showing significant reduction of the CGHAZ hardness relative to the as-welded condition, Fig. 19a, and a small number of very high hardness values in the dissimilar transition zone. Maximin hardness values up to 500 HV_{10} in 8630/FM 625 BS1, 480 HV_{10} in 8630/FM 625 BS3, and 414 HV_{10} in F22/FM 625 DMWs can be related to the planar growth regions and PMxZs in these welds, Fig. 15.

Figure 19c demonstrates the simultaneous effect of base metal composition and PWHT. Compared to the F22 steel, the higher carbon content and lower content of carbide formers in the 8630 steel resulted in up to 150 HV_{10} higher maximum hardness in the 8630/FM 625 dissimilar transition zone.

The high hardness in the dissimilar transition zone, related to formation of M_7C_3 carbides [22] and fresh martensite in PMxZs in post-weld heat-treated 8630/625 DMWs, leads to higher HAC susceptibility than in the F22/FM 625 BS1 weld, Table 6 and Fig. 17. The combined beneficial effects of 1) temper bead welding on formation of stable carbides in the CGHAZ, 2) PHWT on tempering the CGHAZ martensite and 3) base metal composition on lowering the potential for carbon migration during PWHT resulted in high resistance to HAC of the F22/FM 625 BS3 DMW.

The welding and PWHT procedures also affected the hardness in the undiluted FM 625 weld metal, Figs. 16 and 19. BS1 generated harder welds metals than BS3 and PWHT further increased the weld metal hardness. The weld metal hardening is potentially related to the effects of multiple reheats and prolonged exposure to high temperatures on the kinetic of carbides dissolution and precipitation. Clarification of the weld metal hardening mechanisms and their potential effect on the HAC susceptibility in DMWs would require additional investigations.

5 Conclusions

This study established the following criteria for evaluation and ranking HAC susceptibility in DMWs:

1. Conservative criterion for resistance to HAC, defined as no-failure in the delayed hydrogen cracking test (DHCT) for 1,120 h at load equivalent to 90% of the base metal yield strength.
2. Apparent threshold stress for HAC, defined as the maximum stress sustained without failing the DHCT for a duration longer than 1,120 h.

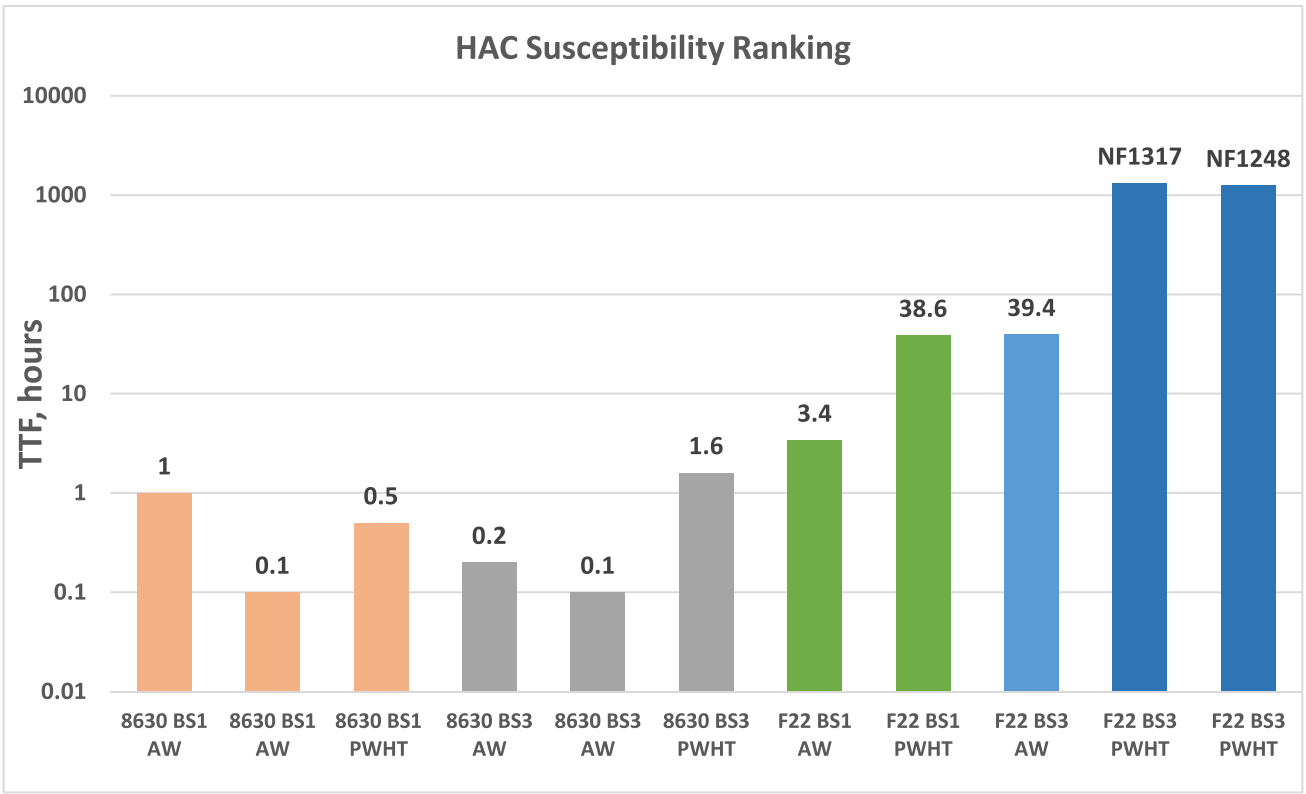

Fig. 17 HAC susceptibility ranking, based on time-to-failure at 90% YS tensile load

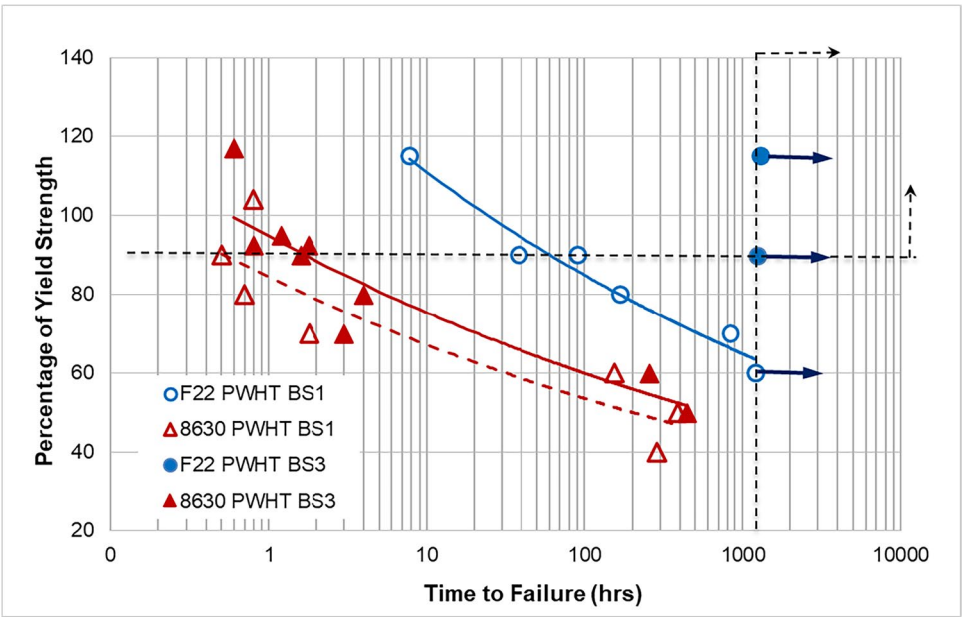

Fig. 18 Percentage of yield strength versus time to failure in all PWHT samples

3. Criterion for ranking HAC susceptibility in DMWs, defined as the time to failure in the DHCT at loads equivalent to 90% of the base metal yield strength.

From all tested DMWs, only PWHT F22/FM 625 BS3 satisfied the HAC resistance criterion. The apparent HAC threshold stress for HAC in the post-weld heat-treated

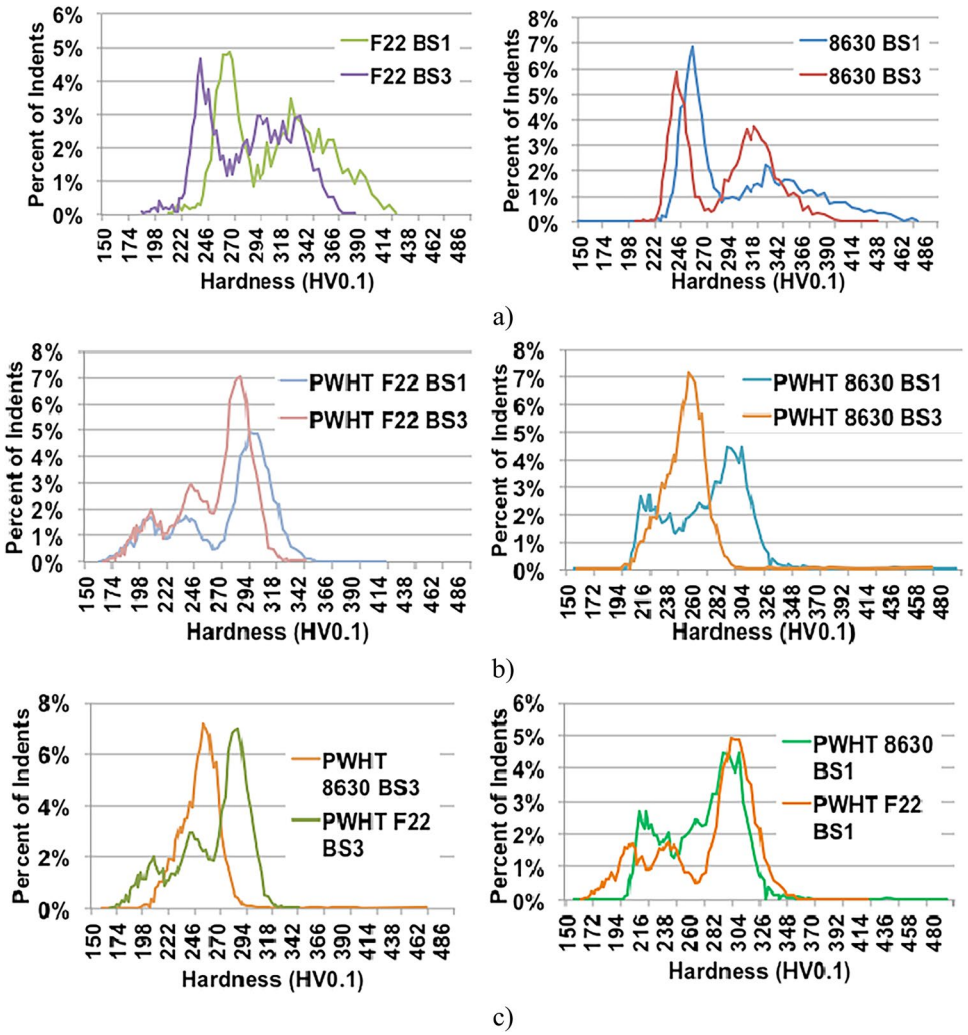

Fig. 19 Effect of controlling factors on hardness distribution in the tested DMWs: **a**) welding procedure, **b**) welding procedure and PWHT, **c**) base metal and PWHT

DMWs was 115%YS in F22/FM 625 BS3, 60%YS in F22/FM 625 BS1, below 50%YS in 8630/FM 625 BS3 and below 40%YS in 8630/FM 625 BS1.

Based on time to failure at 90%YS load, the 8630/FM 625 BS1 and the as-welded 8630/FM 625 BS3 welds were ranked as the most susceptible to HAC, followed by PWHT 8630/FM 625 BS3, as-welded F22/FM 625 BS1, PWHT F22/FM 625 BS1, AW F22/FM 625 BS3, and PWHT F22/FM 625 BS3 as the most resistant to HAC. The apparent threshold stress for HAC generated the equivalent rankings for the post-weld heat-treated DMWs. These rankings fully corresponded to the presence of hard microstructural constituents in the CGHAZ and in the fusion boundary zone of the tested DMWs.

The base metal composition and the welding and PWHT procedures had strong effect on the dissimilar transition zone microstructure, which resulted in times to failure between 0.1 and 893 h and no failure in the DHCT for more than 1,200 h. Due to lower carbon content and higher content of carbide formers in the base metal, the F22/FM 625 DMWs had lower HAC susceptibility than 8630/FM 625 DMWs. PWHT tempered the CGHAZ but generated hard, susceptible to HAC microstructural constituents in the dissimilar transition zone and did not reduce the HAC susceptibility in the 8630/FM 625 DMWs. By tempering the GGHAZ before PWHT, the BS3 welding procedure reduced the negative effect of PWHT on the dissimilar transition zone microstructure.

The results of this study, in terms of wide range of times to failure and apparent threshold stresses for HAC, demonstrated the high sensitivity of the DHCT to the effects of base metal composition and welding and PWHT procedures on the HAC susceptibility in DMWs.

Acknowledgements This work was originally supported by the ExxonMobil Corporation through the NSF I/UCRC for Manufacturing & Materials Joining Innovation Center (Ma^{2}JIC).

Declarations

Conflicts of interest The authors declare that they have no conflict of interest.

References

1. Beachem CD (1972) A new model for hydrogen-assisted cracking (hydrogen 'embrittlement'). Metall Mater Trans B 3(2):441–455. https://doi.org/10.1007/BF02642048
2. Hirth JP (1980) Effects of hydrogen on the properties of iron and steel. Metall Trans A 11(6):861–890
3. Petch NJ (1956) The lowering of fracture-stress due to surface adsorption. Philos Mag 1(4):331–337. https://doi.org/10.1080/14786435608238106
4. Troiano AR (1960) The role of hydrogen and other interstitials in the mechanical behavior of metals. Trans ASM 52:54–80
5. Troiano AR (1962) The influence of hydrogen on the mechanical behaviour of steel. The Iron and Steel Institute, Special report, (73)
6. Zapffe C, Sims C (1941) Hydrogen embrittlement, internal stress and defects in steel. Trans AIME 145(1941):225–271
7. Pyun S-I, Lee H-K (1990) Effect of threshold stress intensity on fracture mode transitions for hydrogen-assisted cracking in AISI 4340 steel. Metall Trans A 21(9):2577–2583
8. Rozenak P, Unigovski Y, Shneck R (2016) Effect of gas tungsten arc welding parameters on hydrogen-assisted cracking of type 321 stainless steel. Metall Mater Trans A 47(5):2010–2023
9. Robertson IM et al (2015) Hydrogen embrittlement understood. Metall Mater Trans B 46(3):1085–1103
10. Sadananda K, Vasudevan A (2011) Review of environmentally assisted cracking. Metall Mater Trans A 42(2):279–295
11. Lynch SP (2013) Mechanisms and kinetics of environmentally assisted cracking: current status, issues, and suggestions for further work. Metall Mater Trans A 44(3):1209–1229
12. Alexandrov BT, Lippold J, Sowards J, Hope A, Saltzmann D (2013) Fusion boundary microstructure evolution associated with embrittlement of Ni–base alloy overlays applied to carbon steel. Weld World 57(1):39–53
13. Beaugrand V, Smith LS, Gittos MF (2009) Subsea dissimilar joints: failure mechanisms and opportunities for mitigation," presented at the CORROSION 2009
14. Beaugrand VC, Smith LS, Gittos MF (2009, January) Hydrogen embrittlement of 8630M/625 subsea dissimilar joints: factors that influence the performance. In: International Conference on Offshore Mechanics and Arctic Engineering, vol 43468, pp 227–236
15. Dodge MF, Dong HB, Milititsky M, Barnett RP, Marques VF, Gittos MF (2012, July) Environment–induced cracking in weld joints in subsea oil and gas systems: Part I. In: International Conference on Offshore Mechanics and Arctic Engineering, vol 44908, pp 305–312
16. Dodge MF, Dong HB, Milititsky M, Barnett RP, Gittos MF (2013, June) Environment-induced cracking in weld joints in subsea oil and gas systems: Part II. In: International Conference on Offshore Mechanics and Arctic Engineering, vol 55355, p V003T03A011
17. Gittos M, Gooch T (1992) The interface below stainless steel and nickel-alloy claddings. Carbon 2:4Cr–1Mo
18. Rowe M, Nelson T, Lippold J (1999) Hydrogen-induced cracking along the fusion boundary of dissimilar metal welds. Weld J-N Y 78:31-s
19. Fenske JA (2010) Microstructure and hydrogen induced failure mechanisms in iron-nickel weldments. University of Illinois at Urbana-Champaign
20. Fenske J, Robertson I, Ayer R, Hukle M, Lillig D, Newbury B (2010) Hydrogen effects on the failure mechanisms in Fe-Ni weldments. Microsc Microanal 16(S2):776–777
21. Fenske JA, Hukle MW, Newbury BD, Gordon JR, Noecker R, Robertson IM (2011, January) Hydrogen induced mechanical property behavior of dissimilar weld metal interfaces. In International Conference on Offshore Mechanics and Arctic Engineering, vol 44359:, pp 509–516
22. Fenske J, Robertson I, Ayer R, Hukle M, Lillig D, Newbury B (2012) Microstructure and hydrogen-induced failure mechanisms in Fe and Ni alloy weldments. Metall Mater Trans A 43(9):3011–3022
23. Dai T, Lippold JC (2018) The effect of postweld heat treatment on hydrogen-assisted cracking of 8630/Alloy 625 overlay. Weld World 62(3):581–599
24. Bourgeois D (2015) Hydrogen assisted crack in dissimilar metal welds for subsea service under cathodic protection (Doctoral dissertation, The Ohio State University)
25. Bourgeois D, Alexandrov B, Lippold J, Fenske J (2016) Metallurgical Factors Influencing the Susceptibility of Hydrogen Assisted Cracking in Dissimilar Metal Welds for Application Under Cathodic Protection. In: Cracking Phenomena in Welds IV, Springer, pp 441–455
26. Alexandrov BT, Shi S, Rodelas JM, Lippold JC (2012) A new test for evaluation of susceptibility to hydrogen assisted cracking in dissimilar metal welds," presented at the CORROSION 2012
27. Boellinghaus T, Hoffmeister H, Middel C (1996) Scatterbands for hydrogen diffusion coefficients in steels having a ferritic or martensitic microstructure and steels having an austenitic microstructure at room temperature. Weld World Soudage Dans Monde 1(37):16–23
28. Buntain RJ, Alexandrov BT, Viswanathan G (2020) Characterization of Interpass Macrosegregation in Narrow Groove Closure Welds Between Low Alloy Steel Pipes with Alloy 625 Filler Metal. Mater Charact 170(2020):110638, pp1–11
29. Bourgeois D, Alexandrov B (2022) Hydrogen-assisted cracking fracture analysis using high-speed camera and delayed hydrogen cracking test. J Fail Anal Prev 1–15
30. Fink C, Alexandrov BT (2017) Effect of post weld heat-treatment on fusion boundary microstructure in dissimilar metal welds for subsea service, materials testing 59(6):547–550
31. Rule J (2019) Evaluation and prediction of hydrogen assisted cracking of dissimilar metal welds. PhD Dissertation, The Ohio State University
32. Kuper MW, Alexandrov BT (2019) Retention of Delta Ferrite in the Heat Affected Zone of Grade 91 Steel Dissimilar Metal Welds. Mater Metall Trans A 50A:2732–2747